Biomedicine & Pharmacotherapy 150 (2022) 113016

Contents lists available at ScienceDirect

Biomedicine & Pharmacotherapy

journal homepage: www.elsevier.com/locate/biopha

In vitro and *in silico* analysis of galanthine from *Zephyranthes carinata* as an inhibitor of acetylcholinesterase

Karina Sierra [a], Jean Paulo de Andrade [b], Luciana R. Tallini [c,d], Edison H. Osorio [e], Osvaldo Yañéz [f,g], Manuel Isaías Osorio [h,i], Nora H. Oleas [j], Olimpo García-Beltrán [e], Warley de S. Borges [k], Jaume Bastida [d], Edison Osorio [a,*], Natalie Cortes [e,*]

[a] *Grupo de Investigación en Sustancias Bioactivas, Facultad de Ciencias Farmacéuticas y Alimentarias, Universidad de Antioquía UdeA, Calle 70 No. 52-21, Medellín, Colombia*
[b] *Núcleo Científico Multidisciplinario, Dirección de Investigación, Universidad de Talca, Campus Lircay, CP 3460000, Talca, Chile*
[c] *Programa de Pós-graduação em Ciências Farmacêuticas, Faculdade de Farmácia, Universidade Federal do Rio Grande do Sul, Av. Ipiranga 2752, 90610-0000 Porto Alegre, Brazil*
[d] *Grup de Productes Naturals, Departament de Biologia, Sanitat i Medi Ambient, Facultat de Farmàcia i Ciències de l'Alimentació, Universitat de Barcelona, Av. Joan XXIII, 27-31, 08028 Barcelona, Spain*
[e] *Facultad de Ciencias Naturales y Matemáticas, Universidad de Ibagué, Carrera 22 calle 67, Ibagué, Colombia*
[f] *Center of New Drugs for Hypertension (CENDHY), Santiago 8380494, Chile*
[g] *Facultad de Ingeniería y Negocios, Universidad de las Américas, Santiago 7500000, Chile*
[h] *Center for Bioinformatics and Integrative Biology (CBIB), Facultad de Ciencias de la Vida, Universidad Andres Bello, Santiago, Chile*
[i] *Facultad de Medicina, Universidad Diego Portales, Santiago, Chile*
[j] *Centro de Investigación de la Biodiversidad y Cambio Climático (BioCamb) e Ingeniería en Biodiversidad y Recursos Genéticos, Facultad de Ciencias de Medio Ambiente, Universidad Tecnológica Indoamérica, Machala y Sabanilla, EC170301 Quito, Ecuador*
[k] *Departamento de Química, Universidade Federal do Espírito Santo, Avenida Fernando Ferrari 514, Goiabeiras, 29075-910 Vitória, Espírito Santo, Brazil*

ARTICLE INFO

Keywords:
Amaryllidaceae alkaloids
Galanthine
Acetylcholinesterase inhibition
Molecular docking
Molecular dynamics

ABSTRACT

Zephyranthes carinata Herb., a specie of the Amaryllidoideae subfamily, has been reported to have inhibitory activity against acetylcholinesterase. However, scientific evidence related to their bioactive alkaloids has been lacking. Thus, this study describes the isolation of the alkaloids of this plant, and their inhibition of the enzymes acetylcholinesterase (eeAChE) and butyrylcholinesterase (eqBuChE), being galanthine the main component. Additionally, haemanthamine, hamayne, lycoramine, lycorine, tazettine, trisphaeridine and vittatine/crinine were also isolated. The results showed that galanthine has significant activity at low micromolar concentrations for eeAChE (IC_{50} = 1.96 μg/mL). The *in-silico* study allowed to establish at a molecular level the high affinity and the way galanthine interacts with the active site of the TcAChE enzyme, information that corroborates the result of the experimental IC_{50}. However, according to molecular dynamics (MD) analysis, it is also suggested that galanthine presents a different inhibition mode that the one observed for galanthamine, by presenting interaction with peripheral anionic binding site of the enzyme, which prevents the entrance and exit of molecules from the active site. Thus, in vitro screening assays plus rapid computer development play an essential role in the search for new cholinesterase inhibitors by identifying unknown bio-interactions between bioactive compounds and biological targets.

1. Introduction

Millions of people around the world have been diagnosed with Alzheimer's disease (AD). Officially, the AD is considered as the fifth-leading cause of death worldwide [1]. AD has a slow onset of almost 20 years before the beginning of symptoms [2], which are characterized by undetectable biochemical changes in the brain eventually leading to death. Although there are several hypotheses to explain the pathogenesis of AD, the cholinergic hypothesis suggests that the symptoms related to the loss of cognitive function could be explained by the decreasing of synaptic acetylcholine (ACh) levels [3]. According to the hypothesis, this neurotransmitter plays a key role in number of cognitive

* Corresponding authors.
E-mail addresses: edison.osorio@udea.edu.co (E. Osorio), natalie.cortes@unibague.edu.co (N. Cortes).

https://doi.org/10.1016/j.biopha.2022.113016
Received 25 February 2022; Received in revised form 15 April 2022; Accepted 19 April 2022
Available online 25 April 2022

functions such as memory, emotional processing and learning processes [4]. These functions are a consequence of the high density of cholinergic synapses in the thalamus, striatum, limbic system and neocortex [5,6]. Therefore, the inhibition of the catabolic process of ACh can improve its levels and counterbalance the typical deficit observed in mnemonic synapsis of patients with AD [3,7].

Acetylcholinesterase (AChE) and butyrylcholinesterase (BuChE) are key enzymes in the cholinergic nervous system. Because of their physiological function of enhancing neurotransmission by hydrolyzing ACh, BuChE and even more AChE have been extensively investigated and targeted for pharmacological intervention [8,9]. This strategy reduce the main symptoms in the patients with AD, improving their life quality and independence [7]. Donepezil, rivastigmine and galanthamine are well-known drugs as inhibitors of AChE and are currently used for the management of AD [3] through the cholinergic mechanism, which does not affect the progression of AD [7,10]. There are studies showing non-neurotransmitter [8,11,12] or catalytic [8,13,14] functions alternative to the cholinergic hypothesis in which AChE has an important role beyond the breakdown of ACh, including participation in inflammation, cell apoptosis, morphogenic and adhesion functions, as well as participation in oxidative stress [4]. In fact, AChE exists as different variants derived from alternative RNA splicing, generating different polypeptide-encoding transcripts, which can also influence protein-protein interactions [15].

The main transcript in the brain encodes subunits that produce monomeric (G1) and tetrameric (G4) forms of AChE [16], while on erythrocytes, the dimeric form (G2) is mainly found [4]. Its active site, however, is conserved and is composed of four main subsites in the bottom gorge: the oxyanion hole, acyl binding pocket, anionic subsite, and catalytic anionic site (CAS) where the hydrolysis of ACh takes place [23]. Outside the protein gorge, the peripheral anionic site (PAS) is located [22] and it has been evidenced that it could promote the deposition and aggregation of Aβ in the brain [17,18]. Thus, inhibition of AChE could disrupt the self-assembly of Aβ plaques, providing a more effective way for the management of AD [19,20]. In addition, understanding the role of each AChE allows an even better understanding of the pathogenesis and pathophysiology of AD, since the particular distribution of each AChE species allows its interaction with specific proteins. Therefore, the evaluation of molecules of interest in each model could change according to the characteristics of each structure [8].

Galanthamine has demonstrated superior response in clinical terms, pharmacokinetics parameters, and reduced toxic effects, in comparison with others AChE inhibitors. This alkaloid is a natural compound found, in significant amount, in several genera of Amaryllidaceae family (particularly Amaryllidoideae subfamily), such as *Narcissus* from Central and West Europe, *Leucojum* from East Europe, *Lycoris* from China, *Hippeastrum* from Brazil, and *Ungernia* from Uzbekistan and Kazakhstan [21]. The therapeutic uses of galanthamine was approved by the Food and Drug Administration (FDA) in 2001 [22], and since then, the search for new AChE inhibitors from species of Amaryllidoideae subfamily have increased substantially [23,24].

Zephyranthes carinata Herb. (*Z. carinata*) from the Amaryllidoideae subfamily is an ornamental species in Colombia, originally described in Mexico [25], that under the edaphoclimatic conditions of the country produces alkaloids of the narciclasine, haemanthamine, lycorine, galanthamine and tazettine type. Their alkaloid-enriched extracts have also shown remarkable AChE inhibitory activity in both, *in vitro* and *in vivo* experiments [26–29]. Interestingly, galanthamine is not a major alkaloid in the plant species. As a continuity of our previous efforts to know the mode of action of the alkaloids of *Z. carinata* evaluated in triple transgenic mice as a model for AD (3xTg-AD) [30], the main compounds of the enriched-alkaloid extracts from bulbs were purified and evaluated in eeAChE, a G4 AChE species from *Electrophorus electricus* [8], and equine butyrylcholinesterase (eqBuChE). Finally, through *in-silico* tools, we analysed how galanthine, the most active alkaloid *in vitro*, interacts with the PAS and anionic subsite sites of AChE.

2. Materials and methods

2.1. Plant material

Z. carinata was collected in Antioquia, Colombia during the flowering period between February and April 2014. A representative specimen (4263 Alzate) was kept in the herbarium of the University of Antioquia (Medellin, Colombia) [31]. The collected plant material was completely dried in oven at 40 °C followed by grind process before extraction. The extraction for obtaining enriched-alkaloid fractions were done under the same parameters of the previous studies [30,31].

2.2. Extraction and isolation

Methanol was used to extract the plant material (about 1800 g of pulverized *Z. carinata* bulbs). The solvent was evaporated under vacuum (rotavapor), and the residue diluted in 2% H_2SO_4 before being defatted with EtOAc. The aqueous layers were then basified with 25% ammonia to a pH of 9.5–10.0 and the alkaloids partitioned with $CHCl_3$. 7.9 g of enhanced alkaloid extract was obtained after four partitioning steps, and 6.0 g was subjected to silica gel column chromatography (CC) ($CHCl_3$-MeOH, 90:10–0:100) to obtain nine fractions (Fr. 1–9). Exclusion Chromatography (EC) was used to separate Fr. 2 (70.0 mg) using Sephadex® LH-20 as the stationary phase and MeOH as the mobile phase, yielding eight fractions (Fr.2A-Fr 0.2 H). Trisphaeridine **(1)** (5.6 mg) precipitated from Fr. 2 H. From the fraction Fr. 3 (520.0 mg), galanthine **(2)** precipitated (119.7 mg). The supernatant from Fr. 3 was processed to Sephadex® LH-20 with MeOH as the mobile phase, yielding nine fractions (Fr. 3A-Fr. 3I). Tazettine **(3)** (33.1 mg) precipitated from the fraction Fr. 3D. The SubFr. 4D was fractionated again using Sephadex® LH-20 (MeOH as mobile phase) and seven additional subfractions (SubFr. 4D-1 – SubFr. 4D-7) were produced. Lycorine **(4)** has been identified as the primary component of SubFr. 4D-2 (2.3 mg). The EC was used again with Sephadex® LH-20 (MeOH as mobile phase) to fractionate the SubFr. 4 F (392.5 mg), resulting in five fractions (Fr.4F1-Fr.4F5) containing haemantamine **(5)** (28.6 mg) precipitated from the Fr.4F3. EC (Sephadex® LH-20, MeOH as mobile phase) was used to separate Fr. 7 (510.0 mg) into ten fractions (Fr. 7 A - Fr. 7 J). Lycoramine **(6)** was isolated from Fr. 7B fraction (20.6 mg). The portion Fr. 7D (33.7 mg) was subjected to preparative thin layer chromatography using a $CHCl_3$:MeOH (8:2) combination as mobile phase, and the alkaloid hamayne was isolated **(7)** (2.6 mg). Finally, fraction Fr. 7 J (16.4 mg) was separated using semi-preparative reverse-phase chromatography (H_2O:ACN:MeOH:CF_3COOH, 80:10:10:0.01) to give vittatine/crinine **(8)** (5.4 mg) with a retention period of 8.0 min

2.3. Preparative HPLC systems

Chromatographic analyses were performed on an Agilent preparative equipment equipped with a binary pump (model G1361A-1260 – California, USA), a 1260 MWD VL detector (model G1365D), and an automated fraction collector (Agilent 1260 FC-PS, model G1364B). The mobile phase was formed of an isocratic system (H_2O:MeOH:ACN, 8:1:1, +0.1% CF_3COOH), while the stationary phase was composed of a semi-preparative Agilent Eclipse XDB-C18 (5 mm, 9.4 mm × 250 mm) column (CA, USA). The flow rate was set to 7 mL min^{-1}. At 270 and 290 nm, the absorbance was determined.

2.4. GC/MS analysis

We used a previously reported approach for capillary gas chromatography/mass spectrometry (GC/MS) analyses [32]. The Agilent 7890 (GC) was utilized in conjunction with an MS running at 70 eV. The column was an HP-1 MS capillary column (30 m x 0.25 mm×0.25 μm). The following temperature program was used: 1 min hold at 120 °C, 120–210 °C at a rate of 15 °C/min, 210–260 °C at a rate of 8 °C/min, and

260–300 °C at a rate of 15 °C/min. The temperature of the injector was 280ºC in splitless mode. The carrier gas (He) rate was 1 mL min^{-1} of flow and 1.0 µL of the solution was injected. The alkaloids were identified by comparing their mass spectral fragmentation to those in the NIST database (NIST Mass Spectral Database, 2008, National Institute of Standardization and Technology, USA) or by comparing their spectra to those described in the literature. An alternative identification of the alkaloids was made by comparing their GC/MS spectra with our in-home library database. This collection has been updated and evaluated on a regular basis using isolated alkaloids that have been reliably identified using physical and spectrometric techniques. The Kovats retention rates (RI) of the compounds were recorded with a mixture of standard calibration n-hydrocarbons (C7 - C40). All the mass spectra were deconvoluted using AMDIS 2.64 (NIST) software.

2.5. Nuclear magnetic resonance (NMR)

We performed mono- and bi-dimensional NMR investigations on a Varian VNMRS 400 MHz (Palo Alto, CA, USA) utilizing CD_3OD and $CDCl_3$ as solvents and TMS as the internal standard. By comparing their NMR spectra to those already published in the literature, the alkaloids were identified.

2.6. eeAChE and eqBuChE inhibitory microplate assay

The quantification of the inhibitory activity of the eeAChE and eqBuChE enzymes were performed according to Ellman et al.(1961) [33] with some modifications [31]. The buffers used in the test were prepared as follows: buffer A, 50 mM Tris - HCl, pH 8.0; buffer B, 50 mM Tris - HCl, pH 8.0 with 0.1% bovine serum albumin in buffer A; and buffer C, 50 mM Tris - HCl, pH 8.0 containing 0.1 M NaCl and 0.02 M $MgCl_2$ - 6 H_2O in buffer A. Alkaloids were prepared in a range of concentrations from 7.5 µg/mL to 240 µg/mL in buffer A, and 25 µL of each solution was added to a 96-well microplate. Subsequently, ATCI or BTCI (25 µL, 15 mM) and DTNB in buffer C (125 µL, 3 mM) along with buffer B (50 µL) were added. The absorbance was measured at 409 nm at a constant temperature of 37 °C using a microplate reader. eeAChE or eqBuChE enzymes were added (25 µL, 0.22 U/mL) and the absorbance was read every 45 s (for 30 min). In this assay, galanthamine was used as a positive control. Any increase in absorbance due to spontaneous hydrolysis of the substrate was corrected by subtracting the absorbance before the addition of the enzyme. The inhibition percentage was calculated using the equation:

$$\text{Inhibition (\%)} = (1 - (\text{A sample/A Control})) \times 100)$$

Where "A sample" represents the absorbance of the sample extract and "A control" represents the absorbance of the blank (DMSO as the dissolving solvent in buffer A (50 mM Tris–HCl, pH 8)). The extract concentration that inhibited 50% of the enzyme (IC_{50}) was determined by plotting the percentage inhibition vs the alkaloid concentration. The values of inhibitory concentration of 50% of the eeAChE and eqBuChE (IC_{50}) were calculated from at least four different concentrations of the sample using the GraphPad Prism 5 statistical package.

2.7. Molecular docking

The term "molecular docking" refers to a technique for predicting the preferred relative orientation of a molecule (or ligand) when it attaches to an active site of a macromolecule and forms a stable complex. When the total system's free energy is reduced, a stable complex is obtained. To acquire the most stable conformations of ligands, the three-dimensional (3D) structures are subjected to a geometrical optimization technique using the Gaussian 09 software [34] at the PBE0 [35]/6–311 +g* [36] level of theory. This approach is effective in confirming structural conformations as real minima on the potential energy surface. The binding mechanism of several alkaloids to the active site of the *Torpedo californica* acetylcholinesterase (TcAChE) protein, PDB code 1DX6 [37], was investigated in this work using the AutoDock v.4.2 tool [38]. This one combines a rapid energy evaluation through pre-calculated grids of affinity potentials, which consisted of a three-dimensional lattice of regularly spaced points centered on some region of interest of the macromolecule under study, with a variety of search algorithm to find suitable binding positions for a ligand on a given macromolecule, where this one is treated as a rigid body. Water molecules, cofactors, and ions are omitted from the X-ray crystallographic structure during protein preparation for docking molecular modeling. Moreover, the polar hydrogen atoms of the enzyme are added, atomic charges were computed toward the Gasteiger procedure and non-polar hydrogen atoms were merged. The grid maps required by AutoDock, one for each atom type present in the docked ligand, were computed using the auxiliary program AutoGrid, which chose a grid box with dimensions of 60 Å × 60 Å × 60 Å around the active site, which is located at the coordinates 3.5, 64.4, and 63.1. The search space was sufficiently large to encompass the most critical active site residues. The Lamarckian Genetic Algorithm (LGA) was used to conduct the docking searches [39]. This technique was used to a population of 2000 persons, resulting in 2,500,000 energy evaluations for each of 200 LGA runs. The best conformations were chosen from the cluster with the maximum number of conformations that had the lowest docked energy solutions. The best docking complex solutions (poses) were analyzed according to the potential intermolecular interactions (ligand/enzyme), such as hydrogen bonding, hydrophobic interactions and the cation–π, π–π stacking.

2.8. Molecular dynamics simulations (MD)

MD calculations were conducted on the complex TcAChE protein (PDBID: 1DX6) in aqueous solutions with the ligands galanthine and galanthamine using an explicit solvent TIP3P water model [40] (≈16.000 water molecules). In addition, Na^+ and Cl^- ions were added to neutralize the systems and maintain an ionic concentration of 0.15 mol L^{-1}. GAFF Force Field (GAFF) was used to parametrize galanthine and galanthamine for organic compounds [41,42]. The protein structures were modeled with the force field ff14SB [43]. The simulations were carried out using a standard MD protocol as follows: (I) Minimization and structural relaxation of water molecules utilizing 2000 stages of minimization (downward step) and MD simulations with an NPT (300 K) assembly by 1000 ps employing harmonic constraints of 10 kcal·mol $Å^{-2}$ on the protein and ligand; (II) minimization of the complete structure considering 2000 downstream minimization steps and 6500 steps of conjugate gradient minimization; (III) the minimized systems were progressively heated to 300 K, with harmonic restrictions of 10 kcal·mol $Å^{-2}$ in the carbon skeleton and ligand during 0.5 ns; (IV) The system was then balanced for 0.5 ns while adhering to the constraints, and then for 5 ns without constraints to 300 K in a canonical assembly (NVT); and (V) a production dynamic was conducted for 50 ns without constraints at 300 K and 1 atm with a temporary passage of 2 fs using an isothermal isobaric assembly (NPT). In the MD simulation, the temperature was controlled by the Langevin dynamics with a collision frequency of 1 ps^{-1} (NVT) and the pressure with the Berendsen barostat (NPT). In addition, the Particle Mesh Ewald (PME) method with a cut-off value of 10 Å was used to treat nonbonding and long-range electrostatic interactions. All MD simulation calculations were performed using the Graphics Processing Unit (GPU)-AMBER Implementations18 [44]. Molecular visualization of the systems and MD trajectory analysis were carried out with the VMD software package [45].

2.8.1. Free energy calculation

The binding free energy of TcAChE-ligand complexes was estimated using the molecular MM/GBSA technique. For computations, the first 40 ns of MD were isolated and the explicit water molecules and ions

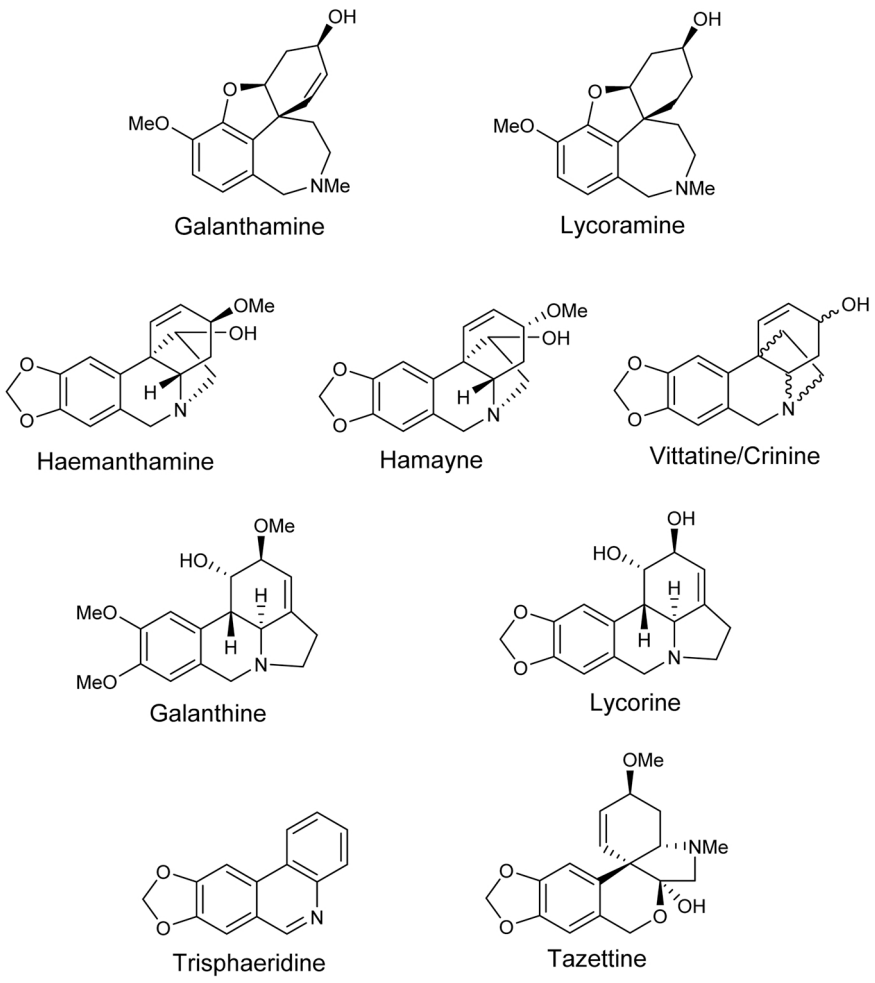

Fig. 1. Purified alkaloids structures.

were deleted. Three subsets of each system were analyzed using MM/GBSA: the protein alone, the ligand alone, and the complex (protein-ligand). The total free energy (ΔGtot) was computed as follows for each of these subsets:

$$\Delta G_{tot} = E_{MM} + G_{Solv} - T\Delta S_{conf}$$

Where E_{MM} denotes the bonded and Lennard–Jones energy components; G_{Solv} denotes the polar and nonpolar contributions to the solvation energy, respectively; T denotes the temperature; and ΔS_{conf} denotes the conformational entropy [46]. Both E_{MM} and G_{Solv} were calculated using AMBER 18 program with the generalized Born implicit solvent model [47,48]. ΔG_{tot} was calculated as a linear function of the solvent-accessible surface area, which was calculated with a probe radius of 1.4 Å [49]. The difference between the binding free energies of TcACh and ligand complexes (ΔG_{bind}) was used to compute the binding free energy of TcACh and ligand complexes (ΔG_{bind}) where values represent the simulation's averages.

$$\Delta G_{bind} = G_{tot}\ (complex) - G_{tot}\ (protein) - G_{tot}\ (ligand)$$

2.8.2. Noncovalent interaction index (NCI)

To reveal possible non-covalent interactions of TcAChE-ligand complexes such as hydrogen bonds, steric repulsion, and van der Waals interactions, the non-covalent interaction index (NCI) [50,51] was used. The NCI is based on the electron density (ρ), its derivatives, and the reduced density gradient (s).

$$s = \frac{1}{2(3\pi^2)^{\frac{1}{3}}} \frac{\nabla\rho}{\rho^{\frac{4}{3}}}$$

In this methodology, non-covalent interactions appear at low electron densities and reduced density gradient values. Thus, the reduced density gradient's isosurface is shown at low values. Weak interactions can thus be seen as closed domains in the molecular space that surround the regions of contact. The blue areas denote strong attractive connections, the green areas denote weak Van der Waals interactions, and the red areas denote a significant non-bonded overlap. In this work, the promolecular densities (ρ^{pro}), computed as the sum of all atomic contributions, were used. The NCI was calculated using the NCIPLOT program [50].

2.9. Statistical analysis

At least three separate tests were used to evaluate experiments. ANOVA was used to examine data with homogeneous variance using the PRISM program. To minimize inter-assay variation, all sample groups were processed in parallel.

3. Results and discussion

3.1. Isolation of alkaloids and their eeAChE and eqBuChE inhibitory activity

Since the first isolation, around 636 structures of isolated or tentatively recognized alkaloids from Amaryllidoideae plants have been

Table 1
IC_{50} values of the alkaloidal fraction and alkaloids isolated against eeAChE and eqBuChE enzymes.

Name	Alkaloid type	eeAChE IC_{50} (μg/mL)	eqBuChE IC_{50} (μg/mL)
Alkaloidal fraction of bulbs	NA	4.26 ± 0.57	57.03 ± 4.06$^{###}$
Lycoramine	Galanthamine	42.48 ± 1.66***	> 60$^{###}$
Haemanthamine	Haemanthamine	44.69 ± 4.79***	> 60$^{###}$
Hamayne	Haemanthamine	50.25 ± 5.06***	> 60$^{###}$
Vittatine/Crinine	Haemanthamine	> 60***	> 60$^{###}$
Galanthine	Lycorine	1.96 ± 0.01	> 60$^{###}$
Lycorine	Lycorine	53.63 ± 11.95***	> 60$^{###}$
Trisphaeridine	Narciclasine	42.07 ± 9.77***	31.91 ± 0.52$^{###}$
Tazettine	Tazettine	29.59 ± 2.36***	> 60$^{###}$
Galanthamine (positive control)	Galanthamine	0.59 ± 0.11	7.53 ± 0.37

Data are expressed as the means ± standard deviation (SD) of at least three independent experiments. ***, **, and * represent significant difference versus control (galanthamine) with AChE. ###, ##, and # represent significant difference versus control (galanthamine) with eqBuChE. $p < 0.001$, $p < 0.002$ or $p < 0.033$, respectively. 2way ANOVA with Dunnett's multiple comparison test (the differences for each component in both eeAChE and eqBuChE inhibition are in relation to the positive control (galanthamine) inhibition for each enzyme).

reported. These different compounds have been classified into 42 Amaryllidaceae skeleton types, being 16 of them the most representative at the different genera [52]. The recognized alkaloids galanthine, haemanthamine, hamayne, lycoramine, lycorine, tazettine, trisphaeridine, and vittatine/crinine were purified in this study, and these results are consistent with prior GC/MS evaluations [30]. However, in this alkaloid extract, haemanthamine and hamayne have not been detected earlier by GC/MS, but they were separated as minor components. The identification of these eight recognized alkaloids (Fig. 1) was based on a comparison of their spectroscopic data to those previously published in the literature [53–55]. Vittatine and crinine are enantiomers and they must be unambiguously assigned using Circular Dichroism, which could not be carried out at this time. The results of inhibition for both enzymes expressed as IC_{50} of each alkaloid are shown in Table 1.

Galanthine had the lowest IC_{50} value (1.96 μg/mL, corresponding to 6.18 μM) for eeAChE with no statistical difference when compared to the positive control galanthamine, which is consistent with previously published findings [26]. The other alkaloids in this model presented IC_{50} values higher than 29.59 μg/mL. The alkaloid galanthine is not commercial and has been consistently determined in many species of *Zephyranthes* [56,57]. Since the 1950 s, this genus has been investigated extensively, yielding significant results not only in terms of alkaloid isolation, but also in terms of dereplication techniques and biological activities [58]. The latter have been particularly focused on AChE enzyme inhibition due to the promising results obtained for this target with enriched-alkaloid extracts from *Zephyranthes* species and their purified components [27–29]. In fact, galanthine was isolated with high extraction performance from *Z. carinata* and showed remarkable activity as AChE inhibitor [26]. Although galanthine has been shown to have biological activity, the inhibitory results vary depending on the experimental settings, since the chemical has been reported to be inactive in some investigations [59], and in others, it is active in the eeAChE model [26]. This information indicates that the alkaloid's mode of action at the active site of the protein is unknown. Additionally, despite the fact that galanthine is ineffective in human model enzymes (dimeric form (G2) found primarily on erythrocytes) [60], the eeAChE model is extensively explored due to its high concentration of the tetrameric form (G4) found in the brain [16].

Trisphaeridine exhibited the most modest inhibition of eqBuChE of all drugs examined. According to the literature, trisphaeridine has a lower molecular docking affinity for BuChE (PDB code: 4BDS) than galanthamine (−8.23 and −7.27 kcal.mol-1, respectively) [61], which is consistent with our data.

3.2. Analysis of molecular docking results

Due to the fact that galanthine has the lowest IC_{50} value for eeAChE, a theoretical inhibition toward molecular docking experiments was undertaken to investigate the inhibition mode of galanthine, using galanthamine as a control. The model used for this experiment was *Tetronarce californica* (an electric ray formerly known as *Torpedo californica*), a classic preparation for biochemical studies of cholinergic neurotransmission [62] and *in silico* model of eeAChE [63]. The results suggested that the estimated free energy of ligand-protein complexes binding was quite near to each other, with galanthine exhibiting − 8.84 kcal.mol-1 and galanthamine exhibiting − 8.78 kcal.mol-1. As a first

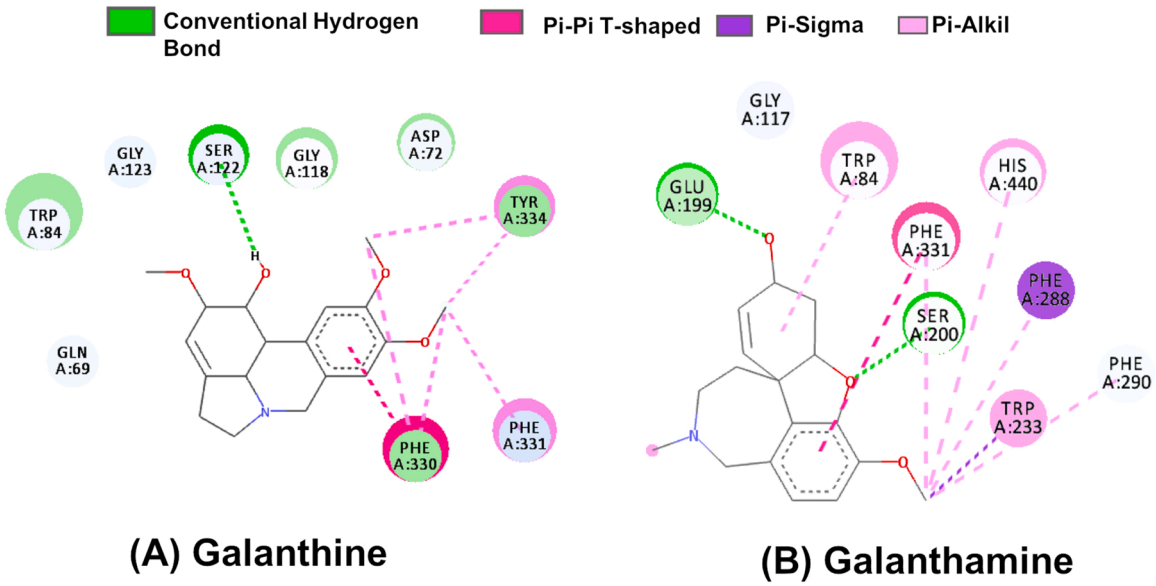

Fig. 2. Principal interactions located by the molecular docking experiments between the ligands (A) Galanthine and (B) Galanthamine with the TcAChE enzyme.

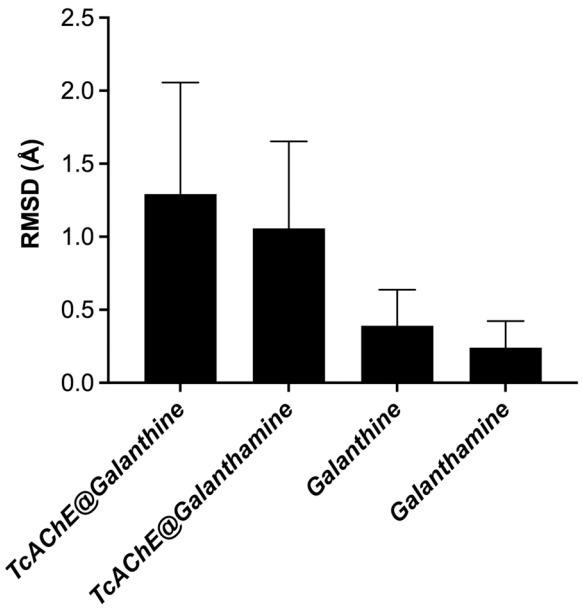

Fig. 3. RMSD calculated for TcAChE backbones, and the ligands used in MD procedures.

Table 2
Free energy calculations of TcAChE in the presence of galanthine and galanthamine.

Substrate	MM-GBSA (kcal·mol^{-1})[a]	Molecular Docking (kcal·mol^{-1})
Galanthine	-35.2 (0.06)	-8.84
Galanthamine	-31.1 (0.06)	-8.78

[a] The values in parentheses correspond to the standard deviation of the energy calculation.

approximation, these data indicate that galanthine is approximately as effective as galanthamine as a TcAChE inhibitor. The most important interactions between the ligands (a) Galanthine and (b) Galanthamine with the TcAChE are presented in Fig. 2.

TcAChE's active site is approximately 20 mm deep and is composed of three distinct regions: i) the peripheral anion site (PAS), which is made of Tyr70, Tyr121, Asp72, Trp279, and Tyr334 residues placed at the active site's gate; and ii) the alpha-anionic site, which is composed of Trp84 and Phe330 residues positioned in the active gorge site. Both residues are aromatic, which allows for stabilization via π-π interactions; and iii) the catalytic anion site (CAS), which is primarily constituted of Ser200, His440, and Glu 327 residues [64,65]. Galanthamine's location in the CAS-ligand complex, near to the catalytic triad, has been extensively documented [66,67]. Our results have once again shown this (Fig. 2B). Our findings for galanthine indicate that there are no stabilizing interactions with Ser200 and His440 residues (Fig. 2A). However, there are several interactions with 4 different amino acids located in different areas of CAS: a stabilizing π-π stacking interactions with Phe330; a hydrogen bonding interaction with Ser122, located at alpha-anionic site; π-Alkil interactions with Tyr334, located at PAS; and π-Alkil interactions with Phe331. Thus, the molecular docking calculus suggests that the inhibition mode of galanthine is different than galanthamine, because galanthine is located in the alpha-anionic and PAS sites.

3.3. Analysis of molecular dynamics (MD) simulation results

MD simulations were conducted using the docking results to elucidate the mechanism by which galanthine inhibits eeAChE. MD simulations were performed to estimate the free energy of binding for both complexes using molecular mechanics generalized Born solvent accessibility (MM-GBSA) calculations. The small values in the root-mean-square deviation (RMSD) study indicate the stability of protein-ligand conformations during MD (Fig. 3).

The binding free energies presented in Table 2 indicate that the galanthine complex is significantly more stable than the galanthamine complex by 4.1 kcal.mol^{-1}. This result corroborates experimental and molecular docking studies indicating that galanthine is as effective as galanthamine as a TcAChE inhibitor. To determine the frequency of interaction between the residues and the alkaloids, we performed a contact frequency study between the most significant residues and the galanthine and galanthamine molecules throughout the MD. A radius of 3 Å was chosen as the assessed region for this research because it corresponds to the average distance between hydrogen bond variations in the analyzed systems. The MD results showed that galanthamine is located at the bottom of the active site, near to the catalytic triad Ser 200, Glu 327, and His 440. Additionally, Fig. 4 demonstrates a significant interaction between galanthamine and the Phe 288 and Phe 290 residues. These amino acids are involved in the formation of the acyl-binding pocket.

The schematic representation of active sites after 60 ns of MD

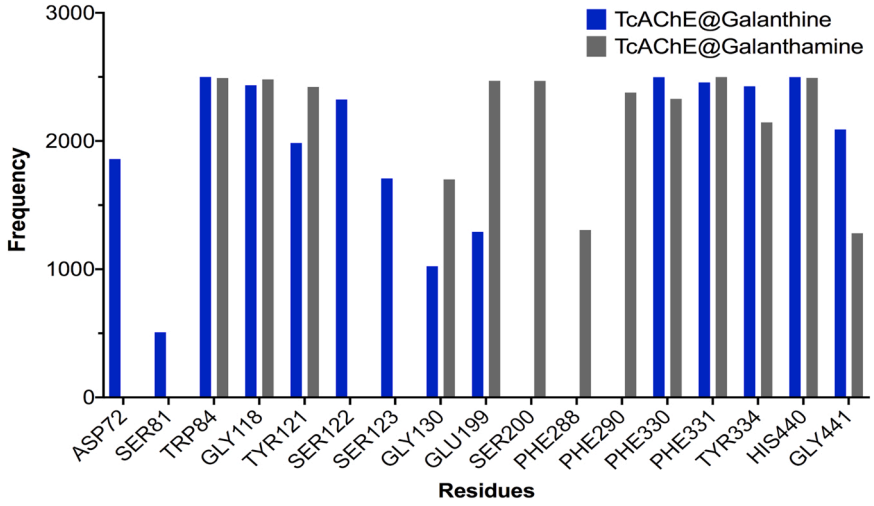

Fig. 4. Frequency of the appearance of residues at a distance of 3 Å or closer from a ligand for TcAChE calculated using MD procedures. The reason of 3 Å was the length of the hydrogen bond ranges from 2.6 Å to 3.1 Å based on observation from the PDB.

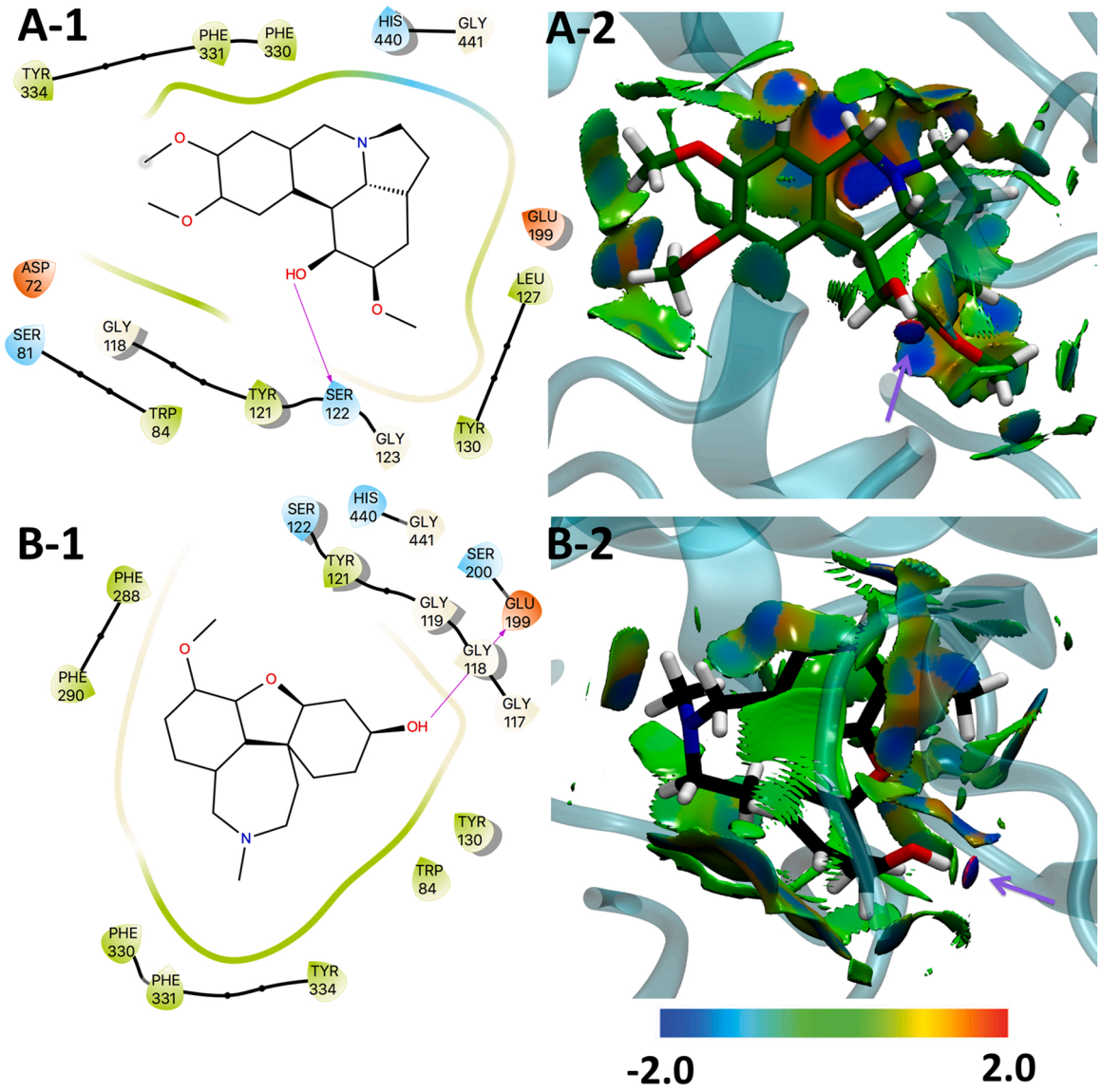

Fig. 5. Schematic representations at the end (60 ns) of their respective production runs for ligands (A) Galanthine and (B) Galanthamine bound to TcAChE. (1) Two-dimensional interaction map of galanthine and galanthamine with TcACh. The arrows indicate potential interactions between amino acid residues and the ligands. (2) NCIPLOT isosurface gradient (0.5 au) of ligands on the structure of TcACh.

simulation is shown in Fig. 5. With regards to the galanthine complex, the MD analysis detects no interactions with Ser 200, Phe 288, or Phe 290 residues, indicating that this ligand is located at a distinct region of the active site's bottom. The most important interactions occur at the peripheral anion site: Asp72, Ser 81, Tyr121 and Ser122 residues (Fig. 5A-1) and PAS: mainly by Phe330 and His440 residues. PAS contributes to the enzyme's catalytic efficiency by trapping substrates or inhibitors on their way to the active site [68]. Additionally, it has been suggested that PAS may facilitate the deposition and aggregation of Aβ in the brain [17,18]. As a result, galanthine coupled to PAS may inhibit Aβ formation and deposition, making it a more effective treatment for AD management [19]. The stabilization of galanthamine (Fig. 5B-1) occurs at the bottom of the active site, near to the catalytic site formed by the Glu199 and Ser200 residues.

The noncovalent interactions are colored according to their strength and kind in the isosurfaces created by the NCIPLOT tool, Figs. 5A-2 and 5B-2. The hues in the spectrum range from blue to red, with blue indicating strong attractive contacts (hydrogen bridges), green indicating moderate or weak attractive interactions (Van der Waals), and red indicating a strong non-binding overlap. There are two regions in galanthine (Fig. 5A-2) that exhibit strong interactions: the stabilization of OH by Ser122 and the interaction of NH with His440. This is insignificant in the case of non-stabilizing interactions in the red zone compared to weak binding interactions in the green region. For galanthamine (Fig. 5B-2), the NCIPLOT analysis reveals a significant interaction caused by the Gly118 residue stabilizing the OH group in direct contact with the catalytic triad Glu199 and Ser200. As is the case with galanthine, the non-binding overlap sections are quite small. Finally, both graphs have a significant region of weak Van der Waals interactions that serve to stabilize both ligands.

4. Conclusions

In summary, it has been demonstrated that *Z. carinata* produces primarily galanthamine-, haemanthamine-, and lycorine-type alkaloids. As the primary component, galanthine was separated. According to the antecedents of enhanced alkaloid fractions from *Zephyranthes* species being effective cholinesterase inhibitors, all separated alkaloids were bio-assayed for their inhibition of the eeAChE and eqBuChE enzymes. Galanthine exhibited substantial activity against eeAChE at low

micromolar doses. The *in-silico* investigation established the high affinity of galanthine and the mechanism by which it interacts with the active site of the TcAChE enzyme at the molecular level. NCIPLOT data indicate that galanthine's interactions with the active site are attractive and stabilizing, which corroborates the experimental result IC_{50}. However, molecular dynamics study suggests that galanthine inhibits the enzyme differently than galanthamine does, by interfering with the enzyme's PAS, preventing molecules from entering and exiting the active site. Thus, *in vitro* screening assays in combination with quick computer development are critical in the hunt for new cholinesterase inhibitors because they enable the discovery of previously unknown bio interactions between bioactive chemicals and biological targets.

Funding

This work was supported by the Universidad de Ibagué Research Fund, Ibague, Colombia, project No. 20-001-INT.

CRediT authorship contribution statement

Karina Sierra: Conceptualization, Methodology, Validation, Formal analysis, Investigation, Writing – original draft. **Jean Paulo de Andrade:** Methodology, Validation, Investigation, Writing – original draft. **Luciana R. Tallini:** Methodology, Validation, Investigation, Writing – original draft. **Edison H. Osorio:** Methodology, Software, Validation, Formal analysis, Investigation, Writing – original draft, Supervision. **Osvaldo Yañez:** Methodology; Software, Validation, Formal analysis, Investigation, Writing – original draft. **Manuel Isaías Osorio:** Methodology, Software, Validation, Formal analysis, Investigation. **Nora H. Oleas:** Resources, Writing – review & editing. **Olimpo García-Beltrán:** Resources, Writing – review & editing. **Warley de S. Borges:** Resources, Writing – review & editing. **Jaume Bastida:** Methodology, Resources, Writing – review & editing. **Edison Osorio:** Conceptualization, Methodology, Resources, Writing – original draft, Project administration, Funding acquisition. **Natalie Cortes:** Conceptualization, Methodology, Validation, Formal analysis, Investigation, Resources, Writing – original draft, Supervision, Project administration, Funding acquisition.

Conflict of interest statement

The authors declare that there is no conflict of interests.

Data Availability

Data will be made available on request.

Acknowledgements

The authors thank to University of Antioquia (UdeA), Colombia, for the contribution in the development of this work. LRT is thankful to CAPES-Brazil (Coordenação de Pessoal de Nível Superior - Bolsista CAPES, processo 13553135) for a doctoral and postdoctoral fellowship.

References

[1] World Health Organization (WHO), The top 10 causes of death, (2018). https://www.who.int/news-room/fact-sheets/detail/the-top-10-causes-of-death (accessed July 24, 2020).
[2] A. Association, 2019 Alzheimer's disease facts and figures, Alzheimer's Dement 15 (2019) 321–387, https://doi.org/10.1016/j.jalz.2019.01.010.
[3] A.A.D.T. Abeysinghe, R.D.U.S. Deshapriya, C. Udawatte, Alzheimer's disease; a review of the pathophysiological basis and therapeutic interventions, Life Sci. 256 (2020), 117996, https://doi.org/10.1016/j.lfs.2020.117996.
[4] Ł.J. Walczak-Nowicka, M. Herbet, Acetylcholinesterase inhibitors in the treatment of neurodegenerative diseases and the role of acetylcholinesterase in their pathogenesis, 2021, Vol. 22, Page 9290, Int. J. Mol. Sci. 22 (2021) 9290, https://doi.org/10.3390/IJMS22179290.
[5] R. Hussain, H. Zubair, S. Pursell, M. Shahab, Neurodegenerative diseases: regenerative mechanisms and novel therapeutic approaches, Brain Sci. 8 (2018) 177, https://doi.org/10.3390/BRAINSCI8090177.
[6] G. Pepeu, C. Grossi, F. Casamenti, The brain cholinergic system in neurodegenerative diseases, Annu. Res. Rev. Biol. 6 (2015) 1–19, https://doi.org/10.9734/ARRB/2015/14623.
[7] G. Marucci, M. Buccioni, D.D. Ben, C. Lambertucci, R. Volpini, F. Amenta, Efficacy of acetylcholinesterase inhibitors in Alzheimer's disease, Neuropharmacology (2020), 108352, https://doi.org/10.1016/j.neuropharm.2020.108352.
[8] M.L. Campanari, M.S. García-Ayllón, O. Belbin, J. Galcerán, A. Lleó, J. Sáez-Valero, Acetylcholinesterase modulates presenilin-1 levels and γ-secretase activity, J. Alzheimers Dis. 41 (2014) 911–924, https://doi.org/10.3233/JAD-140426.
[9] R.M. Lane, S.G. Potkin, A. Enz, Targeting acetylcholinesterase and butyrylcholinesterase in dementia, Int. J. Neuropsychopharmacol. 9 (2006) 101–124, https://doi.org/10.1017/S1461145705005833.
[10] D.D. Li, Y.H. Zhang, W. Zhang, P. Zhao, Meta-analysis of randomized controlled trials on the efficacy and safety of donepezil, galantamine, rivastigmine, and memantine for the treatment of Alzheimer's disease, Front. Neurosci. 13 (2019) 472, https://doi.org/10.3389/FNINS.2019.00472/BIBTEX.
[11] J. Massoulié, J. Sussman, S. Bon, I. Silman, Chapter 15: structure and functions of acetylcholinesterase and butyrylcholinesterase, Prog. Brain Res. 98 (1993) 139–146, https://doi.org/10.1016/S0079-6123(08)62391-2.
[12] P.G. Layer, Nonclassical roles of cholinesterases in the embryonic brain and possible links to Alzheimer disease, Alzheimer Dis. Assoc. Disord. 2 (1995) 29–36, https://doi.org/10.1097/00002093-199501002-00006.
[13] A. Dori, J. Cohen, W.F. Silverman, Y. Pollack, H. Soreq, Functional manipulations of acetylcholinesterase splice variants highlight alternative splicing contributions to murine neocortical development, Cereb. Cortex 15 (2005) 419–430, https://doi.org/10.1093/CERCOR/BHH145.
[14] D. Grisaru, M. Pick, C. Perry, E.H. Sklan, R. Almog, I. Goldberg, E. Naparstek, J. B. Lessing, H. Soreq, V. Deutsch, Hydrolytic and nonenzymatic functions of acetylcholinesterase comodulate hemopoietic stress responses, J. Immunol. 176 (2006) 27–35, https://doi.org/10.4049/JIMMUNOL.176.1.27.
[15] J. Massoulié, The origin of the molecular diversity and functional anchoring of cholinesterases, Neurosignals 11 (2002) 130–143, https://doi.org/10.1159/000065054.
[16] D. Kaufer, A. Friedman, S. Seidman, H. Soreq, Acute stress facilitates long-lasting changes in cholinergic gene expression, Nature 393 (1998) 373–377, https://doi.org/10.1038/30741.
[17] M. Pera, A. Martínez-Otero, L. Colombo, M. Salmona, D. Ruiz-Molina, A. Badia, M. V. Clos, Acetylcholinesterase as an amyloid enhancing factor in PrP82-146 aggregation process, Mol. Cell. Neurosci. 40 (2009) 217–224, https://doi.org/10.1016/J.MCN.2008.10.008.
[18] L. Jean, S. Brimijoin, D.J. Vaux, In vivo localization of human acetylcholinesterase-derived species in a β-sheet conformation at the core of senile plaques in Alzheimer's disease, J. Biol. Chem. 294 (2019) 6253, https://doi.org/10.1074/JBC.RA118.006230.
[19] H. Akrami, B.F. Mirjalili, M. Khoobi, H. Nadri, A. Moradi, A. Sakhteman, S. Emami, A. Foroumadi, A. Shafiee, Indolinone-based acetylcholinesterase inhibitors: synthesis, biological activity and molecular modeling, Eur. J. Med. Chem. 84 (2014) 375–381, https://doi.org/10.1016/J.EJMECH.2014.01.017.
[20] P. Sharma, P. Srivastava, A. Seth, P.N. Tripathi, A.G. Banerjee, S.K. Shrivastava, Comprehensive review of mechanisms of pathogenesis involved in Alzheimer's disease and potential therapeutic strategies, Prog. Neurobiol. 174 (2019) 53–89, https://doi.org/10.1016/J.PNEUROBIO.2018.12.006.
[21] S. Berkov, L. Georgieva, V. Kondakova, A. Atanassov, F. Viladomat, J. Bastida, C. Codina, Plant sources of galanthamine: phytochemical and biotechnological aspects, Biotechnol. Biotechnol. Equip. 23 (2009) 1170–1176, https://doi.org/10.1080/13102818.2009.10817633.
[22] M. Heinrich, Chapter 4 – galanthamine from galanthus and other amaryllidaceae – chemistry and biology based on traditional use, Alkaloids Chem. Biol. (2010) 157–165, https://doi.org/10.1016/S1099-4831(10)06804-5.
[23] S. Berkov, J. Bastida, F. Viladomat, C. Codina, Analysis of galanthamine-type alkaloids by capillary gas chromatography–mass spectrometry in plants, Phytochem. Anal. 19 (2008) 285–293, https://doi.org/10.1002/pca.1028.
[24] M.N. Akram, R. Verpoorte, B. Pomahačová, Methods for the analysis of galanthamine and its extraction from laboratory to industrial scale, South Afr. J. Bot. 136 (2021) 51–64, https://doi.org/10.1016/j.sajb.2020.08.004.
[25] F. Alzate, M. Lesmes, N. Cortés, S. Varela, E. Osorio, Sinopsis de la familia Amaryllidaceae en Colombia, Biota Colomb. 20 (2019) 2–20, https://doi.org/10.21068/c2019.v20n01a01.
[26] G. Zhan, J. Zhou, J. Liu, J. Huang, H. Zhang, R. Liu, G. Yao, Acetylcholinesterase inhibitory alkaloids from the whole plants of zephyranthes carinata, J. Nat. Prod. 80 (2017) 2462–2471, https://doi.org/10.1021/acs.jnatprod.7b00301.
[27] Cortés Sierra, Borges Tallini, Bastida Andrade, Amaryllidaceae Durango, Alkaloids from zephyrantes carinata and their evaluation as cholinesterases (AChE and BChE) inhibitors, Proceedings 22 (2019) 66, https://doi.org/10.3390/proceedings2019022066.
[28] N. Cortes, R.A. Posada-Duque, R. Alvarez, F. Alzate, S. Berkov, G.P. Cardona-Gómez, E. Osorio, Neuroprotective activity and acetylcholinesterase inhibition of five Amaryllidaceae species:a comparative study, Life Sci. 122 (2015) 42–50, https://doi.org/10.1016/j.lfs.2014.12.011.
[29] N. Cortes, R. Alvarez, E.H. Osorio, F. Alzate, S. Berkov, E. Osorio, Alkaloid metabolite profiles by GC/MS and acetylcholinesterase inhibitory activities with binding-mode predictions of five Amaryllidaceae plants, J. Pharm. Biomed. Anal. 102 (2015) 222–228, https://doi.org/10.1016/j.jpba.2014.09.022.

[30] N. Cortes, A.M. Sabogal-Guaqueta, G.P. Cardona-Gomez, E. Osorio, Neuroprotection and improvement of the histopathological and behavioral impairments in a murine Alzheimer's model treated with Zephyranthes carinata alkaloids, Biomed. Pharmacother. 110 (2019) 482–492, https://doi.org/10.1016/J.BIOPHA.2018.12.013.
[31] N. Cortes, K. Sierra, F. Alzate, E.H. Osorio, E. Osorio, Alkaloids of amaryllidaceae as inhibitors of cholinesterases (AChEs and BChEs): an integrated bioguided study, Phytochem. Anal. 29 (2018) 217–227, https://doi.org/10.1002/pca.2736.
[32] N. Cortes, C. Castañeda, E.H. Osorio, G.P. Cardona-Gomez, E. Osorio, Amaryllidaceae alkaloids as agents with protective effects against oxidative neural cell injury, Life Sci. 203 (2018) 54–65, https://doi.org/10.1016/j.lfs.2018.04.026.
[33] G.L. Ellman, K.D. Courtney, V. Andres, R.M. Feather-Stone, A new and rapid colorimetric determination of acetylcholinesterase activity, Biochem. Pharm. 7 (1961) 88–95. ⟨http://www.ncbi.nlm.nih.gov/pubmed/13726518⟩. accessed November 7, 2013.
[34] C. Adamo, V. Barone, Toward reliable density functional methods without adjustable parameters: The PBE0 model, J. Chem. Phys. 110 (1999) 6158–6170, https://doi.org/10.1063/1.478522.
[35] R. Krishnan, J.S. Binkley, R. Seeger, J.A. Pople, Self-consistent molecular orbital methods. XX. A basis set for correlated wave functions, J. Chem. Phys. 72 (1980) 650–654, https://doi.org/10.1063/1.438955.
[36] D.J.F.M.J. and, G.W. Frisch, H.B. Trucks, G.E. Schlegel, M.A. Scuseria, J.R. Robb, G. Cheeseman, V. Scalmani, G.A. Barone, H. Petersson, X. Nakatsuji, M. Li, A. Caricato, J. Marenich, B.G. Bloino, R. Janesko, B. Gomperts, H.P. Mennucci, J.V. Ort Hratchian, Gaussian 09. Revision E. 01, Gaussian, 2016.
[37] H.M. Greenblatt, G. Kryger, T. Lewis, I. Silman, J.L. Sussman, Structure of acetylcholinesterase complexed with (−)-galanthamine at 2.3 Å resolution, FEBS Lett. 463 (1999) 321–326, https://doi.org/10.1016/S0014-5793(99)01637-3.
[38] G.M. Morris, R. Huey, W. Lindstrom, M.F. Sanner, R.K. Belew, D.S. Goodsell, A. J. Olson, AutoDock4 and AutoDockTools4: automated docking with selective receptor flexibility, J. Comput. Chem. 30 (2009) 2785–2791, https://doi.org/10.1002/jcc.21256.
[39] G.M. Morris, D.S. Goodsell, R.S. Halliday, R. Huey, W.E. Hart, R.K. Belew, A. J. Olson, Automated docking using a Lamarckian genetic algorithm and an empirical binding free energy function, J. Comput. Chem. 19 (1998) 1639–1662, https://doi.org/10.1002/(SICI)1096-987X(19981115)19:14<1639::AID-JCC10>3.0.CO;2-B.
[40] E. Neria, S. Fischer, M. Karplus, Simulation of activation free energies in molecular systems, J. Chem. Phys. 105 (1996) 1902–1921, https://doi.org/10.1063/1.472061.
[41] J. Wang, R.M. Wolf, J.W. Caldwell, P.A. Kollman, D.A. Case, Development and testing of a general amber force field, J. Comput. Chem. 25 (2004) 1157–1174, https://doi.org/10.1002/jcc.20035.
[42] G.A. ÖzpInar, W. Peukert, T. Clark, An improved generalized AMBER force field (GAFF) for urea, J. Mol. Model. 16 (2010) 1427–1440, https://doi.org/10.1007/s00894-010-0650-7.
[43] R. Salomon-Ferrer, D.A. Case, R.C. Walker, An overview of the Amber biomolecular simulation package, Wiley Interdiscip. Rev. Comput. Mol. Sci. 3 (2013) 198–210, https://doi.org/10.1002/wcms.1121.
[44] D.J. Mermelstein, C. Lin, G. Nelson, R. Kretsch, J.A. McCammon, R.C. Walker, Fast and flexible gpu accelerated binding free energy calculations within the amber molecular dynamics package, J. Comput. Chem. 39 (2018) 1354–1358, https://doi.org/10.1002/jcc.25187.
[45] W. Humphrey, A. Dalke, K. Schulten, VMD: visual molecular dynamics, J. Mol. Graph. 14 (1996) 33–38, https://doi.org/10.1016/0263-7855(96)00018-5.
[46] J. M, G. Archontis, MM-GB(PB)SA Calculations of Protein-Ligand Binding Free Energies : Mol. Dyn. - Stud. Synth. Biol. Macromol., InTech 2012 doi: 10.5772/37107.
[47] L.F. Song, T.S. Lee, D.M. Chun-Zhu, K.M. York, Merz, Validation of AMBER/GAFF for relative free energy calculations, ChemRxiv (2019), https://doi.org/10.26434/chemrxiv.7653434.v1.
[48] A.W. Götz, M.J. Williamson, D. Xu, D. Poole, S. Le Grand, R.C. Walker, Routine microsecond molecular dynamics simulations with AMBER on GPUs. 1. generalized born, J. Chem. Theory Comput. 8 (2012) 1542–1555, https://doi.org/10.1021/ct200909j.
[49] H. Abroshan, H. Akbarzadeh, G.A. Parsafar, Molecular dynamics simulation and MM-PBSA calculations of sickle cell hemoglobin in dimer form with Val, Trp, or Phe at the lateral contact, J. Phys. Org. Chem. 23 (2010) 866–877, https://doi.org/10.1002/poc.1679.
[50] J. Contreras-García, E.R. Johnson, S. Keinan, R. Chaudret, J.P. Piquemal, D. N. Beratan, W. Yang, NCIPLOT: a program for plotting noncovalent interaction regions, J. Chem. Theory Comput. 7 (2011) 625–632, https://doi.org/10.1021/ct100641a.
[51] E.R. Johnson, S. Keinan, P. Mori-Sánchez, J. Contreras-García, A.J. Cohen, W. Yang, Revealing noncovalent interactions, J. Am. Chem. Soc. 132 (2010) 6498–6506, https://doi.org/10.1021/ja100936w.
[52] S. Berkov, E. Osorio, F. Viladomat, J. Bastida, Chemodiversity, chemotaxonomy and chemoecology of Amaryllidaceae alkaloids, in: Alkaloids Chemistry and Biology, Academic Press Inc, 2020, pp. 113–185, https://doi.org/10.1016/bs.alkal.2019.10.002.
[53] J. Bastida, R. Lavilla, F. Viladomat, Chapter 3 chemical and biological aspects of narcissus alkaloids, Alkaloids: Chem. Biol. (2006) 87–179, https://doi.org/10.1016/S1099-4831(06)63003-4.
[54] F. Viladomat, C. Codina, J. Bastida, S. Mathee, W.E. Campbell, Further alkaloids from Brunsvigia josephinae, Phytochemistry 40 (1995) 961–965, https://doi.org/10.1016/0031-9422(95)00375-H.
[55] F. Viladomat, J. Bastida, C. Codina, W.E. Campbell, S. Mathee, Alkaloids from Boophane flava, Phytochemistry 40 (1995) 307–311, https://doi.org/10.1016/0031-9422(95)00191-9.
[56] E. Kohelová, J. Maříková, J. Korábečný, D. Hulcová, T. Kučera, D. Jun, J. Chlebek, J. Jenčo, M. Šafratová, M. Hrabinová, A. Ritomská, M. Malaník, R. Peřinová, K. Breiterová, J. Kuneš, L. Nováková, L. Opletal, L. Cahlíková, Alkaloids of Zephyranthes citrina (Amaryllidaceae) and their implication to Alzheimer's disease: Isolation, structural elucidation and biological activity, Bioorg. Chem. 107 (2021), 104567, https://doi.org/10.1016/j.bioorg.2020.104567.
[57] J. del, C. Rojas-Vera, A.A. Buitrago-Díaz, L.M. Possamai, L.F.S.M. Timmers, L. R. Tallini, J. Bastida, Alkaloid profile and cholinesterase inhibition activity of five species of Amaryllidaceae family collected from Mérida state-Venezuela, South Afr. J. Bot. 136 (2021) 126–136, https://doi.org/10.1016/j.sajb.2020.03.001.
[58] K.D. Singh, B. S. B, Phytochemistry and pharmacology of genus zephyranthes, Med. Aromat. Plants 04 (2015) 1–8, https://doi.org/10.4172/2167-0412.1000212.
[59] B.S. Jensen, S.B. Christensen, A.K. Jäger, N. Rønsted, Amaryllidaceae alkaloids from the Australasian tribe Calostemmateae with acetylcholinesterase inhibitory activity, 2011. http://www.sciencedirect.com/science/article/pii/S030519781100024X (accessed November 6, 2013).
[60] D. Hulcová, J. Maříková, J. Korábečný, A. Hošťálková, D. Jun, J. Kuneš, J. Chlebek, L. Opletal, A. De Simone, L. Nováková, V. Andrisano, A. Růžička, L. Cahlíková, Amaryllidaceae alkaloids from Narcissus pseudonarcissus L. cv. Dutch Master as potential drugs in treatment of Alzheimer's disease, Phytochemistry 165 (2019), https://doi.org/10.1016/J.PHYTOCHEM.2019.112055.
[61] L.R. Tallini, J. Bastida, N. Cortes, E.H. Osorio, C. Theoduloz, G. Schmeda-Hirschmann, Cholinesterase inhibition activity, alkaloid profiling and molecular docking of chilean rhodophiala (Amaryllidaceae), Molecules 23 (2018), https://doi.org/10.3390/molecules23071532.
[62] M. Stavrianakou, R. Perez, C. Wu, M.S. Sachs, R. Aramayo, M. Harlow, Draft de novo transcriptome assembly and proteome characterization of the electric lobe of Tetronarce californica: a molecular tool for the study of cholinergic neurotransmission in the electric organ, BMC Genom. 18 (2017) 611, https://doi.org/10.1186/S12864-017-3890-4/TABLES/6.
[63] J. Lindstrom, J. Cooper, S. Tzartos, Acetylcholine receptors from Torpedo and Electrophorus have similar subunit structures, Biochemistry 19 (2002) 1454–1458, https://doi.org/10.1021/BI00548A029.
[64] I. Silman, J.L. Sussman, Acetylcholinesterase: how is structure related to function? Chem. Biol. Interact. 175 (2008) 3–10, https://doi.org/10.1016/j.cbi.2008.05.035.
[65] H. Dvir, I. Silman, M. Harel, T.L. Rosenberry, J.L. Sussman, Acetylcholinesterase: from 3D structure to function, Chem. Biol. Interact. 187 (2010) 10–22, https://doi.org/10.1016/j.cbi.2010.01.042.
[66] C. Pilger, C. Bartolucci, D. Lamba, A. Tropsha, G. Fels, Accurate prediction of the bound conformation of galanthamine in the active site of Torpedo californica acetylcholinesterase using molecular docking11Color Plates for this article are on pages 374–378, J. Mol. Graph. Model 19 (2001) 288–296. ⟨http://www.sciencedirect.com/science/article/pii/S1093326300000565⟩. accessed November 8, 2013.
[67] J. Correa-Basurto, M. Bello, M.C. Rosales-Hernández, M. Hernández-Rodríguez, I. Nicolás-Vázquez, A. Rojo-Domínguez, J.G. Trujillo-Ferrara, R. Miranda, C. A. Flores-Sandoval, QSAR, docking, dynamic simulation and quantum mechanics studies to explore the recognition properties of cholinesterase binding sites, Chem. Biol. Interact. 209 (2014) 1–13, https://doi.org/10.1016/j.cbi.2013.12.001.
[68] I. Silman, J.L. Sussman, Acetylcholinesterase: how is structure related to function? Chem. Biol. Interact. 175 (2008) 3–10, https://doi.org/10.1016/J.CBI.2008.05.035.